Table-Top Laser-Based Source of Femtosecond, Collimated, Ultrarelativistic Positron Beams

G. Sarri,[1] W. Schumaker,[2] A. Di Piazza,[3] M. Vargas,[2] B. Dromey,[1] M. E. Dieckmann,[1] V. Chvykov,[2] A. Maksimchuk,[2] V. Yanovsky,[2] Z. H. He,[2] B. X. Hou,[2] J. A. Nees,[2] A. G. R. Thomas,[2] C. H. Keitel,[3] M. Zepf,[1,4] and K. Krushelnick[2]

[1]*School of Mathematics and Physics, The Queen's University of Belfast, BT7 1NN Belfast, United Kingdom*
[2]*Center for Ultrafast Optical Science, University of Michigan, Ann Arbor, Michigan 48109-2099, USA*
[3]*Max-Planck-Institut für Kernphysik, Saupfercheckweg 1, 69117 Heidelberg, Germany*
[4]*Helmholtz Institute Jena, Fröbelstieg 3, 07743 Jena, Germany*

(Received 20 December 2012; published 20 June 2013)

The generation of ultrarelativistic positron beams with short duration ($\tau_{e^+} \simeq 30$ fs), small divergence ($\theta_{e^+} \simeq 3$ mrad), and high density ($n_{e^+} \simeq 10^{14}$–10^{15} cm^{-3}) from a fully optical setup is reported. The detected positron beam propagates with a high-density electron beam and γ rays of similar spectral shape and peak energy, thus closely resembling the structure of an astrophysical leptonic jet. It is envisaged that this experimental evidence, besides the intrinsic relevance to laser-driven particle acceleration, may open the pathway for the small-scale study of astrophysical leptonic jets in the laboratory.

DOI: 10.1103/PhysRevLett.110.255002 PACS numbers: 52.38.Kd, 25.20.−x, 98.58.Fd

Relativistic positron beams are of paramount importance in experimental physics due to their direct application to a wide range of physical subjects, including nuclear physics, particle physics, and laboratory astrophysics. Arguably, the most practical way to generate them is to exploit the electromagnetic cascade initiated by the propagation of an ultrarelativistic electron beam through a high-Z solid. This process is exploited to generate low-energy positrons in injector systems for conventional accelerators such as the Electron-Positron Collider (LEP) [1]. In this case, an ultrarelativistic electron beam ($E_{e^-} \approx$ 200 MeV) was preaccelerated by a LINAC and then directed onto a tungsten target. The resulting positron population was further accelerated by a large-scale ($R \approx 27$ km), synchrotron accelerator up to 209 GeV. The large cost and size of these machines have motivated the study of alternative particle accelerator schemes. In particular, laser-plasma devices (overall size of a few tens of meters) can support accelerating fields of the order of 100s of gigavolts/meter, much higher than typical megavolts/meter in solid-state accelerators. Laser-driven electron beams with energies per particle reaching [2–5], and exceeding [6] 1 GeV have been experimentally demonstrated and the production of electron beams with energies approaching 100 GeV is envisaged for the next generation of high-power lasers (1–10 PW) [7]. Hybrid schemes have also been proposed and successfully tested in first proof-of-principle experiments [8,9]. On the other hand, laser-driven low energy positrons ($E_{e^+} \approx$ 1–5 MeV) have been first experimentally obtained by C. Gahn and coworkers [10] and recently generated exploiting picosecond, kilojoule class lasers [11–14]. Despite the intrinsic interest of these results, the low energy and broad divergence reported ($E_{e^+} \leq 20$ MeV and $\theta_{e^+} \geq 350$ mrad, respectively) still represent clear limitations for future use in hybrid machines.

The possibility of generating high density and high energy electron-positron beams is of central importance also for astrophysics due to their similarity to jets of long gamma-ray bursts [15]. These structures still present enigmatic features which are virtually impossible to address by simply relying on direct observations. A possible solution might be represented by reproducing small scale electron-positron jets (required bulk flow Lorentz factor of the order of 100–1000) in the laboratory. Although gamma-ray burst jets may have a weak large scale magnetic field [16], the external shock is exclusively mediated by self-generated microscale magnetic fields. A purely electronic jet would present toroidal magnetic fields whose strength and structure would be comparable to the microscale fields that develop in response to the filamentation instability [17] and modify the shock physics. The presence of the highly mobile positrons would reduce the overall magnetization of the jet, simplifying the interpretation of the experimental data and their comparison with the astrophysical scenario.

Here we experimentally demonstrate the possibility of producing collimated and high-density ultrarelativistic positron beams in a fully laser-driven configuration. Their low divergence and short duration (comparable to those of the incoming laser-driven electron beam) suggest the possibility of applying this generation scheme to current laser facilities towards the construction of a fully optical generator of high-quality, ultrarelativistic positron beams. Furthermore,the measured high positron Lorentz factors ($\gamma_{e^+} \simeq 200$–300, compared to $\gamma_{e^+} \leq 40$ in Refs. [10–12]) of these beams are finally comparable to those of astrophysical leptonic jets. This, in conjunction with the low divergence, the inferred electron-positron balance, and co-propagation with intense gamma-rays, finally opens up a realistic possibility of studying the dynamics of such jets in the laboratory.

 © 2013 American Physical Society

The experiment [shown schematically in Fig. 1(a)] was carried out using the HERCULES laser system at the Center for Ultrafast Optical Science at the University of Michigan [18], which delivered a laser beam with a central wavelength $\lambda_L = 0.8$ μm, energy $E_L = 0.8$ J, and duration $\tau_L = 30$ fs. This laser beam was focused, using an $f/20$ off-axis parabola, onto the edge of a 3 mm wide supersonic He gas jet, doped with 2.5% of N_2, with a backing pressure of 5.5 bar. Once fully ionized, this corresponds to an electron density of 9×10^{18} cm^{-3}. The focal spot size was measured to have a radius of 23 μm which contained 50% of the laser energy (peak intensity of $I_L \approx 6 \times 10^{18}$ W/cm^2). Laser power and gas-jet pressure were chosen in order to stay slightly above the threshold for ionization injection [19]. This interaction delivered a reproducible electron beam with a divergence at full width at half maximum of approximately 1.4 mrad (corresponding to a full width at total maximum of 2.5 mrad [see Figs. 1(b) and 1(c), and Fig. 1 of the Supplemental Material [20]]). Its spectrum was measured, prior to any shot with a high-Z solid target, by a magnetic spectrometer consisting of a 0.8 T, 15 cm long pair of magnets and a LANEX screen. The arrangement of the spectrometer did not allow us to resolve electron energies below 80 MeV. Typical spectra, obtained using the calibration curves reported in Ref. [21], indicated the charge carried by electrons with energy exceeding 80 MeV to be of the order of 50 pC (3×10^8 electrons). Electron bunches obtained in similar conditions have been shown to have a length comparable to a plasma wavelength ($\lambda_{pe} = 2\pi c/\omega_{pe} \approx 10$ μm) implying a typical temporal duration comparable to that of the laser pulse [22]. The laser-accelerated electron beam interacted with millimeter-size high-Z solid targets of different materials (Cu, Sn, Ta, Pb) and thicknesses (from 1.4 to 6.4 mm). The same magnetic spectrometer was used to separate the electrons from the positrons which were then recorded onto an image plate (IP). In order to minimize the effect of the shot-to-shot fluctuation of the electron beam, each IP was exposed to ten consecutive shots [see Fig. 1(b) for the signal on the IP for 4.2 mm of Ta]. Due to the small difference in positron and electron stopping power (below 2% [23]), the signal recorded was absolutely calibrated by using the calibration curves reported in Ref. [24]. Plastic and Teflon shielding were inserted to reduce the noise on the IP induced by both the low-energy electrons and gamma rays generated, at wide angles, during the laser-gas and electron-solid target interactions [see Fig. 1(a)].

In these experimental conditions, the positrons inside the high-Z target are mainly generated via either direct electroproduction (trident process), in which pair production is mediated by a virtual photon in the electron field [25], or via a two-step "cascade" process where the electron first emits a real photon (bremsstrahlung) [26], which then produces an electron-positron pair via the Bethe-Heitler process [27]. Keeping the parameters of the electron beam constant, the positron yield N_{e^+} is expected to scale as $N_{e^+} \propto (Z^2 n d)^j$, where n is the number of atoms per unit volume in the material, d is the thickness of the solid target, and $j = 1$ for the trident process and $j = 2$ for the two-step cascade process (we neglect here Coulomb corrections, which depend on $Z\alpha$, with $\alpha \approx 1/137$ being the fine-structure constant). Neglecting the difference between the proton and the neutron mass, the mass density of the solid target is $\rho \approx A m_p n$, with A and m_p being the atomic number and the proton mass, respectively. If we maintain the areal mass density ($\sigma = \rho d$) constant, we can then express the scaling as $N_p \propto (Z^2/A)^j$. We have thus performed a series of shots for different materials (Cu, Sn, Ta, Pb) adjusting the target thickness so that the areal mass density was kept constant for each material ($\sigma \approx 4.7$ g/cm^2, see the first four rows in Table I). All the measured positron spectra presented a monotonically decreasing profile with approximately 10^3 positrons/MeV (solid lines in Fig. 2). In all cases, numerical simulations performed with the nuclear physics Monte-Carlo code FLUKA, which accounts for electromagnetic cascades during the passage of an electron beam through a solid target [28], are able to reproduce the experimental data

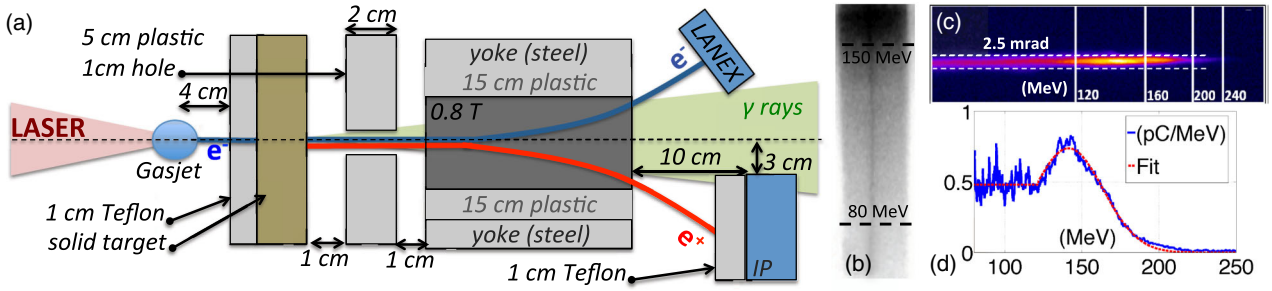

FIG. 1 (color online). (a) Top view of the experimental setup. The magnet is rotated by 90° for the sake of illustration. (b) Typical positron signal as recorded by the image plate for 4.2 mm of Ta. The dark region on the upper part is predominantly exposed by the γ rays escaping the solid target. (c) Typical signal of the electron beam as recorded on the LANEX screen, without a solid target (see Fig. 1 of the Supplemental Material [20] for a ten-shot series). The dashed white lines depict a full width at total maximum of 2.5 mrad (corresponding full width at half maximum of 1.4 mrad). (d) Extracted spectrum and relative best fit (linear + Gaussian) used as an input for FLUKA simulations.

TABLE I. The first four rows illustrate the results from targets with the same areal density. The positron yield N_{exp} and N_{sim} refer to the energy window $90 < E_{e^+}(\mathrm{MeV}) < 120$ as obtained from the experiment and FLUKA simulation, respectively. N_T refers instead to the total yield of positrons with $E_{e^+} > 1$ MeV, as extracted from matching numerical simulations. For each material, the positron divergence refers to the higher section of the positron spectrum (see Fig. 1 of the Supplemental Material [20]).

Mat.	d (mm)	θ_{e^+} (mrad)	$N_{\mathrm{exp}} \times 10^5$	$N_{\mathrm{sim}} \times 10^5$	$N_T \times 10^5$
Cu	5.3	2.3 ± 0.2	0.3 ± 0.1	0.3	31
Sn	6.4	2.7 ± 0.3	0.6 ± 0.1	0.6	63
Ta	2.8	2.7 ± 0.3	2.1 ± 0.3	2.1	190
Pb	4.2	3.5 ± 0.4	2.3 ± 0.3	2.3	240
Ta	1.4	2.3 ± 0.2	0.8 ± 0.2	0.8	78
Ta	4.2	2.7 ± 0.3	3.8 ± 0.3	3.9	350
Pb	2.2	3.0 ± 0.3	0.7 ± 0.2	0.7	60
Pb	2.8	3.3 ± 0.3	1.1 ± 0.3	1.1	122

well (dashed lines in Fig. 2). As an input for the simulation 10^6 electrons with a spectral shape like the one depicted in Fig. 1(c) were used. An average over five identical runs was performed for each material in order to minimize any stochastic error arising from the random seed generator of the code. As theoretically predicted, the positron yield increases for materials with higher atomic number. This trend is quantitatively confirmed by integrating the experimental spectra in the range $90 < E_{e^+}(\mathrm{MeV}) < 120$ (see Table I and Fig. 3). Within this energy range, a maximum positron number of $(2.30 \pm 0.28) \times 10^5$ is obtained for the material with the highest Z (Pb). Fitting the data keeping j as a free parameter, we obtain a best fit for $j = 2.1 \pm 0.1$ confirming the dominance of the cascade process with respect to the trident one [see Fig. 3(b)]. The positron yield over the entire positron spectrum, as extracted from matching FLUKA simulations (N_T in Table I), is seen to follow a similar trend. A further indication as to what process

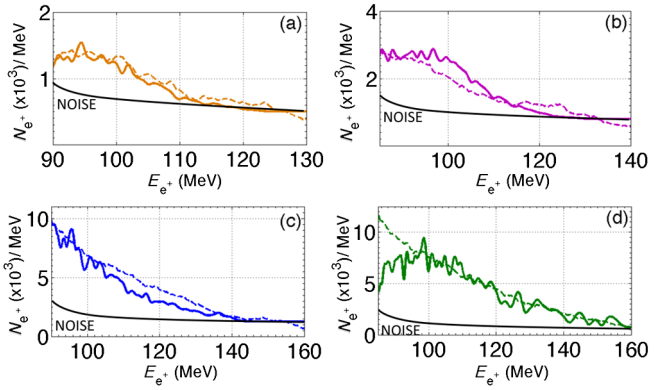

FIG. 2 (color online). Experimental (solid lines) and simulated (dashed lines) positron spectra for (a) 5.3 mm of Cu, (b) 6.4 mm of Sn, (c) 2.8 mm of Ta, and (d) 4.1 mm of Pb. Each experimental spectrum results from an average over ten consecutive shots.

dominates is given by the dependence of the positron yield upon the target thickness ($N_{e^+} \propto d$ for the trident and $N_{e^+} \propto d^2$ for the two-step process). A series of shots was thus taken varying the thickness of the solid target d for Ta and Pb [second four rows in Table I and Fig. 3(a)]. As expected, the positron yield scales with d^2 in both cases. In order to support this statement theoretically, we compare, for each material, the radiation length L_{rad} with the range of target thicknesses d used in the experiment. The two-step process is expected to dominate the trident one if $d/L_{\mathrm{rad}} \gtrsim 10^{-2}$ [25]. For an order-of magnitude estimate of L_{rad}, we can assume here to be in the total-screening regime which, for an electron with energy ε emitting a photon with energy $\hbar\omega$, occurs if the parameter $S \equiv \alpha Z^{1/3}\varepsilon(\varepsilon - \hbar\omega)/(\hbar\omega mc^2)$ is much larger than unity (a Thomas-Fermi model of the atom is assumed [29]). Estimating $\varepsilon \sim \hbar\omega \sim 100$ MeV, we have $S \gtrsim 4$ in the worst case of Cu, which is sufficiently large for the present estimate. In this regime, and by including Coulomb corrections, the radiation length is approximately given by [29] $L_{\mathrm{rad}} \approx 1/[4\alpha(Z\alpha)^2 n\lambda_C^2 L_0]$, where n is the number of atoms per unit volume, $\lambda_C = \hbar/mc = 3.9 \times 10^{-11}$ cm is the Compton wavelength, and $L_0 = \log(183Z^{-1/3}) - f(Z\alpha)$, with $f(x) = \sum_{\ell=1}^{\infty} x^2/\ell(\ell^2 + x^2)$. This gives $L_{\mathrm{rad}}(\mathrm{Cu}) = 15$ mm, $L_{\mathrm{rad}}(\mathrm{Sn}) = 12$ mm, $L_{\mathrm{rad}}(\mathrm{Ta}) = 4.1$ mm, and $L_{\mathrm{rad}}(\mathrm{Pb}) = 5.6$ mm. The material thicknesses are thus always such that the inequality $d/L_{\mathrm{rad}} \gtrsim 10^{-2}$ is fulfilled, in agreement with the experimental indication of the predominance of a two-step process for the electromagnetic cascade. Moreover, in all the considered cases, except one where $d = 4.2$ mm for Ta, it is the case that $d < L_{\mathrm{rad}}$, which implies that the contribution of higher-order cascade processes can generally be neglected for an

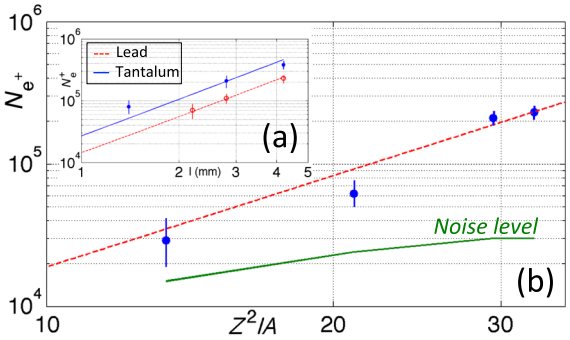

FIG. 3 (color online). (a) Measured positron yield, in the energy range $90 < E_{e^+}(\mathrm{MeV}) < 120$ for Ta (blue full circles) and Pb (red empty circles) for different target thicknesses. Lines give the best quadratic fits. (b) Measured positron yield, in the energy range $90 < E_{e^+}(\mathrm{MeV}) < 120$, for different materials but constant areal density as a function of Z^2/A. The dashed line represents the best quadratic fit. In both graphs, the values result from an average over ten consecutive shots and the error bars account for the shot-to-shot fluctuation of the primary electron beam ($\leq 10\%$ in overall charge, see Fig. 1 of the Supplemental Material [20]).

order-of-magnitude estimate. This is also corroborated by the observed angular divergence θ_{e^+} of the positron beams inferred from the transverse thickness of the positron trace on the IP detector (see the third column in Table I). In fact, according to QED [29], in our experimental conditions, θ_{e^+} is expected to be of the order of $1/\gamma_{e^-}$, with $\gamma_{e^-} \approx 300$ being the relativistic factor of the incoming electron beam.

Due to the divergence of the positron beam, its maximum density is located at the close vicinity of the rear side of the solid target. Here, the positron beam has a transverse diameter of the order of 150 μm and, by assuming that the positron beam will retain the temporal duration of the initial electron beam ($\tau_{e^-} \leq 30$ fs, [22]), a longitudinal length of the order of $c\tau_{e^-} \lesssim 10$ μm. In the case of maximum yield (4.2 mm Ta, see Table I) the density of positrons with an energy between 90 and 120 MeV is of the order of 2.3×10^{12} cm^{-3}. FLUKA simulations indicate that this energy window contains approximately 1% of the total positron yield. For 4.2 mm of Ta, this means that the total number of positrons with energy $E_{e^+} > 1$ MeV will be of the order of 3.5×10^7, indicating an overall positron density of about 2×10^{14} cm^{-3}. The overall positron beam intensity can thus be estimated to be of the order of 10^{19} erg s^{-1} cm^{-2}. FLUKA simulations show that such a positron beam co-propagates with an electron beam with an average density of about $n_{e^-} \approx 2 \times 10^{15}$ cm^{-3}. The positron contribution on the leptonic beam will therefore be of the order of 10% with a null component of positive ions.

We compare now our experimental results with the electron-positron astrophysical jets. Even though a debate is still open as to whether these jets are predominantly constituted by an electron-proton plasma or by electron-positron pairs, an element in favor to the latter is the power-law continuum spectra of the gamma-ray bursts associated with these structures [30]. Despite the different generation mechanism (pair production from gamma-gamma instead of gamma-nucleus collisions), their composition would be similar to the jets reported here, also thanks to their co-propagation with a high-density gamma-ray beam of similar size and duration (FLUKA simulations indicate a gamma-ray brilliance of the order of 10^{19}–10^{20} ph/s/mm^2/mrad^2/0.1%BW). For our experimental parameters, the excess of electrons in the beam implies a net current density of the order of $J_e \approx -(n_e^- - n_e^+)ec \approx -10^{11}$ A/m^2 (assuming $n_e \approx 2 \times 10^{15}$ cm^{-3}) inducing an azimuthal magnetic field of the order of $|B_\phi| \approx 30$ T. However, FLUKA simulations indicate that, by varying the electron beam characteristics and target thickness, it is possible to significantly modify this percentage. For instance, the interaction of a 1 nC, giga-electron-volt-like electron beam with a thicker tantalum target ($d \approx 2$ cm) is expected to generate a high-density, purely neutral electron-positron jet with a leptonic density of 10^{16}–10^{17} cm^{-3}. In this case, the toroidal magnetic fields would be virtually zero, allowing one to unveil the microphysics induced by the presence of small-scale magnetic fields generated by filamentation instability [17]. The high leptonic density would in fact allow for the laboratory study of the propagation of astrophysical jets in the interstellar medium.

The proposed mechanism for the generation of ultrarelativistic positron beams, applied to the near-term developments in laser technology, might also be relevant to the construction of all-optical electron-positron colliders. FLUKA simulations of the interaction of a pencil-like monoenergetic electron beam ($E_{e^-} = 100$ GeV, overall charge of 1 nC, see Ref. [7]) with a 2 cm thick Ta target indicate the production of a positron beam with an exponentially decreasing energy spectrum (maximum energy of $E_{e^+} = 80$ GeV, with approximately 10^6 positrons with energy between 70 and 80 GeV), a divergence of the order of $\theta_{e^+} \approx 10$ μrad, and an overall charge comparable to that of the incoming electron beam. Plasma wakefield accelerators can also be subsequently employed to increase the positron energy in a meter-scale device [8]. The low-divergence achievable with our generation mechanism would prove fundamental for efficient injection of the positrons into such devices. The normalized emittance of such a positron beam can be estimated as $\varepsilon_n \approx \gamma_{e^+}\zeta_{e^+}\theta_{e^+}$, where γ_{e^+}, ζ_{e^+}, and θ_{e^+} are the typical values of the Lorentz factor, of the transversal size, and of the divergence of the positron beam itself. The experimentally measured divergence of the positron beam and corresponding simulations with FLUKA (see Fig. 2 of the Supplemental Material [20]) indicate that the product $\gamma_{e^+}\theta_{e^+}$ is of the order of 1 rad independently of the positron energy. Thus, it results that $\varepsilon_n \sim \zeta_{e^+}$ rad $\approx 30\pi$ mm mrad, in the conservative case of a 100 micron source transversal size. This is comparable to the positron emittance measured after the injection stage of LEP ($\varepsilon_{\mathrm{LEP}} \approx 60\pi$ mm mrad [31]). It must also be noted that the positron beam would be inherently synchronized with the laser, allowing for the possibility of both electron-laser and positron-laser interactions. Direct comparison between these two experimental scenarios might allow for the testing of possible matter or antimatter asymmetries in a highly nonlinear regime.

The authors acknowledge the funding schemes NSF CAREER (Grant No. 1054164) and NSF/DNDO (Grant No. F021166). G. S. wishes to acknowledge the support from the Leverhulme Trust (Grant No. ECF-2011-383). A. D. P. is grateful to A. I. Milstein and to A. B. Voitkiv for stimulating discussions.

[1] R. Bossart *et al.*, Report No. CERN-PS-90-56-LP (1990).
[2] S. Kneip *et al.*, Phys. Rev. Lett. **103**, 035002 (2009).
[3] W. P. Leemans, B. Nagler, A. J. Gonsalves, Cs. Tóth, K. Nakamura, C. G. R. Geddes, E. Esarey, C. B. Schroeder, and S. M. Hooker, Nat. Phys. **2**, 696 (2006).
[4] N. A. M. Hafz *et al.*, Nat. Photonics **2**, 571 (2008).

[5] O. Lundh *et al.*, Nat. Phys. **7**, 219 (2011).
[6] X. Wang *et al.*, AIP Conf. Proc. **1507**, 341 (2012).
[7] W. Lu, M. Tzoufras, C. Joshi, F. Tsung, W. Mori, J. Vieira, R. Fonseca, and L. Silva, Phys. Rev. ST Accel. Beams **10**, 061301 (2007).
[8] I. Blumenfeld *et al.*, Nature (London) **445**, 741 (2007).
[9] P. Muggli *et al.*, Phys. Rev. Lett. **93**, 014802 (2004).
[10] C. Gahn, G. D. Tsakiris, G. Pretzler, K. J. Witte, C. Delfin, C.-G. Wahlstrom, and D. Habs, Appl. Phys. Lett. **77**, 2662 (2000); C. Gahn, G. D. Tsakiris, G. Pretzler, K. J. Witte, P. Thirolf, D. Habs, C. Delfin, and C.-G. Wahlstrom, Phys. Plasmas **9**, 987 (2002).
[11] H. Chen, S. Wilks, J. Bonlie, E. Liang, J. Myatt, D. Price, D. Meyerhofer, and P. Beiersdorfer, Phys. Rev. Lett. **102**, 105001 (2009).
[12] H. Chen *et al.*, Phys. Rev. Lett. **105**, 015003 (2010).
[13] C. Müller and C. H. Keitel, Nat. Photonics **3**, 245 (2009).
[14] A. Di Piazza, C. Müller, K. Z. Hatsagortsyan, and C. H. Keitel, Rev. Mod. Phys. **84**, 1177 (2012).
[15] S. E. Woosley, Astrophys. J. **405**, 273 (1993); T. Piran, Phys. Rep. **314**, 575 (1999).
[16] K. Wiersema *et al.*, Mon. Not. R. Astron. Soc. **426**, 2 (2012).
[17] M. V. Medvedev and A. Loeb, Astrophys. J. **526**, 697 (1999).
[18] V. Yanovsky *et al.*, Opt. Express **16**, 2109 (2008).
[19] C. E. Clayton *et al.*, Phys. Rev. Lett. **105**, 105003 (2010).
[20] See Supplemental Material at http://link.aps.org/supplemental/10.1103/PhysRevLett.110.255002 for ten spectra of the laser-accelerated electron beam, as recorded on the LANEX screen, before the insertion of the solid target (Fig. 1) and for the product between the Lorentz factor and the divergence of the positron beam, as a function of the positron energy, for 4.2 mm of Ta (Fig. 2).
[21] Y. Glinec, J. Faure, A. Guemnie-Tafo, V. Malka, H. Monard, J. P. Larbre, V. De Waele, J. L. Marignier, and M. Mostafavi, Rev. Sci. Instrum. **77**, 103301 (2006).
[22] S. P. D. Mangles *et al.*, Phys. Rev. Lett. **96**, 215001 (2006).
[23] F. Rohrlich and B. C. Carlson, Phys. Rev. **93**, 38 (1954).
[24] K. A. Tanaka, T. Yabuuchi, T. Sato, R. Kodama, Y. Kitagawa, T. Takahashi, T. Ikeda, Y. Honda, and S. Okuda, Rev. Sci. Instrum. **76**, 013507 (2005).
[25] V. N. Baier and V. M. Katkov, Pis'ma Zh. Eksp. Teor. Fiz. **88:2**, 88 (2008).
[26] H. W. Koch and J. Motz, Rev. Mod. Phys. **31**, 920 (1959).
[27] W. Heitler, *The Quantum Theory of Radiation* (Clarendon, Oxford, 1954).
[28] G. Battistoni, F. Cerutti, A. Fasso, A. Ferrari, S. Muraro, J. Ranft, S. Roesler, and P. R. Sala, AIP Conf. Proc. **896**, 31 (2007).
[29] V. B. Beresteskii, E. M. Lifshitz, and L. P. Pitaevskii, *Quantum Electrodynamics* (Butterworth-Heinemann, Oxford, 2008).
[30] M. Hoshino, J. Arons, Y. A. Gallant, and A. B. Langdon, Astrophys. J. **390**, 454 (1992).
[31] J. P. Potier and L. Rinolfi, 6th European Particle Accelerator Conference, Stockholm, Sweden, pp. 859–861 (1998).